PROTEINS
STRUCTURE ■ FUNCTION ■ BIOINFORMATICS

Protein–protein interactions at an enzyme–substrate interface: Characterization of transient reaction intermediates throughout a full catalytic cycle of *Escherichia coli* thioredoxin reductase

Ana Negri,[1] David Rodríguez-Larrea,[2] Esther Marco,[1] Antonio Jiménez-Ruiz,[3] José M. Sánchez-Ruiz,[2] and Federico Gago[1]*

[1] Departmento de Farmacología, Universidad de Alcalá, E-28871 Alcalá de Henares, Madrid, Spain
[2] Departamento de Química Física, Facultad de Ciencias, Universidad de Granada, E-18071 Granada, Spain
[3] Departmento de Bioquímica y Biología Molecular, Universidad de Alcalá, E-28871 Alcalá de Henares, Madrid, Spain

ABSTRACT

A large collection of structural snapshots along a full catalytic cycle of *Escherichia coli* thioredoxin reductase (TrxR) has been generated and characterized using a combination of theoretical methods. Molecular models were built starting from the available X-ray crystallographic structures of dimeric wild-type TrxR in the flavin-oxidizing conformation and a C135S TrxR mutant enzyme in a flavin-reducing conformation "trapped" by a cross-link between Cys138 of TrxR and Cys32 of C35S mutant thioredoxin (Trx). The transition between these two extreme states, which is shown to be reproduced in a normal mode analysis, as well as natural cofactor binding and dissociation, were simulated for the wild-type species using unrestrained and targeted molecular dynamics following docking of oxidized Trx to reduced TrxR. The whole set of simulations provides a comprehensive structural framework for understanding the mechanism of disulfide reduction in atomic detail and identifying the most likely intermediates that facilitate entry of NADPH and exit of $NADP^+$. The crucial role assigned to Arg73 and Lys36 of Trx in substrate binding and complex stabilization was ascertained when R73G, R73D, and K36A site-directed mutants of Trx were shown to be impaired to different extents in their ability to be reduced by TrxR. On the basis of previous findings and the results reported herein, *E. coli* TrxR appears as a beautifully engineered molecular machine that is capable of synchronizing cofactor capture and ejection with substrate binding and redox activity through an interdomain twisting motion.

Proteins 2010; 78:36–51.

Key words: protein–protein interactions; thioredoxin reductase; thioredoxin; molecular dynamics; differential scanning calorimetry.

INTRODUCTION

Escherichia coli TrxR (EC 1.6.4.5),[1] a representative member of a large family of thiol-disulfide oxidoreductases,[2] uses the isoalloxazine ring of its flavin adenine dinucleotide (FAD) prosthetic group to shuttle reducing equivalents from the nicotinamide adenine dinucleotide phosphate (NADPH) cofactor to a redox-active disulfide bridge (reductive half-reaction). In a second step, the two resulting thiols are used to reduce the disulfide present in the oxidized form of Trx (oxidative half-reaction). The binding sites for FAD and NADPH in TrxR reside in different domains, each of which contains the characteristic βαβ nucleotide-binding motif, and both domains are connected by a short stretch made up of two antiparallel β-strands (Fig. 1).

In common with glutathione reductase (GR), the structural parent of the family, *E. coli* TrxR is dimeric but, in contrast with GR, lacks a C-terminal interface domain. Besides, the active-site cysteine (Cys) residues of both enzymes (CATC in TrxR and CVNVGC in GR) do not align in the primary sequence and are in fact located in different domains. This poses an interesting problem for *E. coli* TrxR because the same face of the FAD flavin ring system that is used to stack the nicotinamide ring of NADPH and yield $FADH_2$ (the so-called *re* face) is then employed for electron transfer to the active-site disulfide, which is present in the NADPH-binding domain.[1] On

Additional Supporting Information may be found in the online version of this article.
Dedicated to our late colleague and friend Angel R. Ortiz.
The authors state no conflict of interest.
Grant sponsor: PharmaMar (Colmenar Viejo, Madrid); Grant sponsor: Comisión Interministerial de Ciencia y Tecnología; Grant number: SAF2006-12713-C02-02; Grant sponsor: Comunidad de Madrid; Grant number: S-BIO/0214/2006.
Ana Negri's current address is Department of Structural and Chemical Biology, Mount Sinai School of Medicine, New York, NY 10029-657, USA
*Correspondence to: Federico Gago, Departmento de Farmacología, Universidad de Alcalá, E-28871 Alcalá de Henares, Madrid, Spain. E-mail: federico.gago@uah.es
Received 27 February 2009; Revised 19 May 2009; Accepted 20 May 2009
Published online 2 June 2009 in Wiley InterScience (www.interscience.wiley.com).
DOI: 10.1002/prot.22490

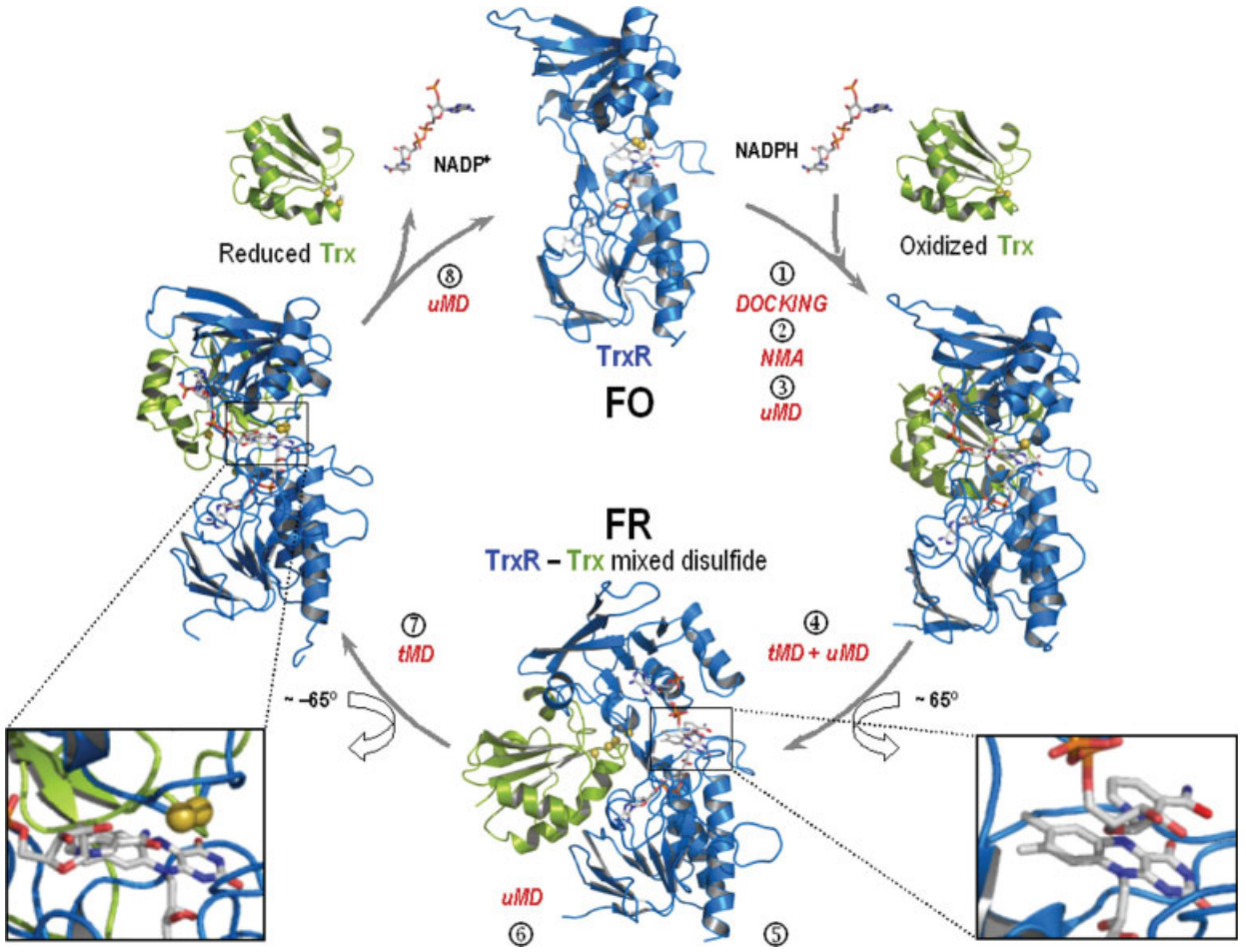

Figure 1

Catalytic cycle of *E. coli* thioredoxin reductase (TrxR) displaying selected structural snapshots of the enzyme (for simplicity only one monomer is shown) in the different redox and conformational states. FO and FR refer to the two extreme conformations of TrxR that allow flavin oxidation and reduction, respectively. Points of entry/exit of the reduced/oxidized cofactor and substrate are indicated by arrows. tMD and uMD stand for targeted and unrestrained molecular dynamics simulations, respectively. The enlarged framed areas show details of the cofactor immediately before flavin reduction (right) and when it starts leaving this site as $NADP^+$ to allow positioning of the incoming disulfide (bonded yellow spheres) over the flavine.

the contrary, in GR,[3] as well as in mammalian TrxR,[4] the disulfide is placed under the opposite face of the flavin (the so-called *si* face) so that hydride transfer, first from NADPH to FAD and then from $FADH_2$ to the cystine, is possible in the absence of large conformational changes.[5] In both cases, however, transfer will occur only at or near nuclear configurations for which the total potential energy of the reactants and surrounding medium is equal to that of the products and surrounding medium, that is, at the intersection between the multidimensional potential energy surfaces describing both states, as formulated in Marcus theory of electron transfer[6] and pointed out by one of the reviewers. Thermal fluctuations of the nuclear coordinates as well as solvent reorganization are necessary to reach this region.

Detailed structural insight into the mechanism of *E. coli* TrxR catalysis was gained initially when the structures of the wild-type enzyme and a Cys138Ser mutant were determined experimentally in the flavin-oxidizing conformation (FO) and refined at 2–2.3 Å resolution.[7,8] It was then found that (i) the active-site disulfide lies adjacent to the buried flavin, in the same location that is used by the nicotinamide ring of NADPH in GR, and (ii) no obvious path exists for the flow of electrons from the nicotinamide ring of the bound pyridine nucleotide in one domain (found only in the Cys138Ser mutant and in an oxidized form)[8] to the FAD prosthetic group in the other domain because the ring systems are separated by ~17 Å (FO in Fig. 1). On the other hand, it was clear that this positioning would facilitate reduction of the di-

sulfide by the flavin of $FADH_2$, although it was not immediately obvious how the reduced Cys residues could then be made accessible to an externally bound Trx molecule. The explanation that was advanced, on the basis of similarities with GR and lipoamide dehydrogenase, was that for the nascent redox-active dithiol to become exposed on the surface of TrxR and be able to interact with the disulfide of oxidized Trx (Trx_{ox}) it would be necessary for the NADPH domain to rotate relative to the FAD-binding domain. It was noted, by inspection of the crystallographic structure, that no barriers to this proposed rotation exist that cannot be surmounted by adjustment of side-chains.[7] This insightful interpretation found direct support when the structure of a Cys135Ser mutant enzyme in a flavin-reducing (FR) conformation "trapped" by a cross-link between Cys138 of TrxR and Cys32 of a Cys35Ser mutant Trx was solved by X-ray crystallography at 2.95 Å resolution and displayed the expected conformation (FR in Fig. 1).[9] This complex showed remarkably little distortion of the local structure of each binding partner and confirmed that switching between the two conformations involves a "ball-and-socket" motion by means of which the pyridine nucleotide-binding and the FAD-binding globular domains rotate by about 70° relative to each other, the swivel being the interconnecting antiparallel β-strand. Another very interesting feature of this complex is that the pyridine ring of 3-amino-pyridine adenine dinucleotide phosphate (AADP), the nonreducing $NADP^+$ analog in whose presence the crystals were grown, is found stacked against the flavin ring. It was surmised, therefore, that a similar binding orientation for NADPH would enable the conversion of FAD to $FADH_2$.

It is then clear that a full catalytic cycle by TrxR, with FAD mediating first NADPH oxidation and then disulfide reduction, requires the enzyme to alternate between the FO and FR conformations and cycle between two electron-reduced (EH_2) and four electron-reduced (EH_4) forms.[10] The FO state allows flavin oxidation by the disulfide, whereas the FR conformation allows flavin reduction by NADPH. The EH_2 form is actually a solution equilibrium between $TrxR(SH)_2$—FAD and TrxR(S—S)—$FADH_2$ microstates. To gain insight into the EH_4 intermediate, which can be described as $TrxR(SH)_2$—$FADH_2$, crystals of *E. coli* TrxR in the FO form were treated with sodium dithionite.[11] Reduction of the isoalloxazine ring resulted in the expected butterfly bending of the flavin,[12] which is planar in the oxidized form, and the active site residues Cys135 and Cys138 indeed appeared as thiols[13] but the protein structure displayed only small local conformational changes, most likely because of the spatial restrictions imposed by the crystal lattice. The recent resolution of both oxidized and dithionite-reduced *Helicobacter pylori* TrxR complexed with $NADP^+$ has provided a similar picture and also additional information about cofactor binding.[14] Finally, the only other structure of prokaryotic NADPH-dependent TrxR solved by X-ray crystallography to date is that from *Mycobacterium tuberculosis*, which has been determined in the FO state at 3 Å resolution and also showed two interacting monomers in the asymmetric unit.[15] Interestingly, this latter work revealed that the NADPH-binding domain, which displayed large anisotropic disorder, was slightly rotated (by ~11°) relative to the FAD-binding domain when compared with that of *E. coli* TrxR in the FO state. Another significant finding was that three single normal modes (but mostly just one) dominated the transition from the experimental conformation to a modeled FR state that reproduced the conformation found for *E. coli* TrxR in the trapped complex with Trx.

Despite the wealth of valuable information provided by all of these experimental structures, none of them actually corresponds to any of the biochemically relevant intermediates of the reaction catalyzed by TrxR.[16] Cys→Ser mutations notwithstanding, the FR conformation, which allows hydride transfer from NADPH to the flavin, was cocrystallized with AADP and has an oxidized flavin. On the other hand, the enzyme found in the FO conformation represents a fully oxidized state that is not part of the catalytic cycle and contains an $NADP^+$ molecule bound in a nonproductive mode (reported attempts to soak NADPH into the crystal resulted in cracking)[8], whereas the fully reduced $TrxR(SH)_2$—$FADH_2$ system (obtained upon chemical reduction of crystals of TrxR in the FO state) is not in the conformation that is biochemically relevant for catalysis (EH_4 in Fig. 2).

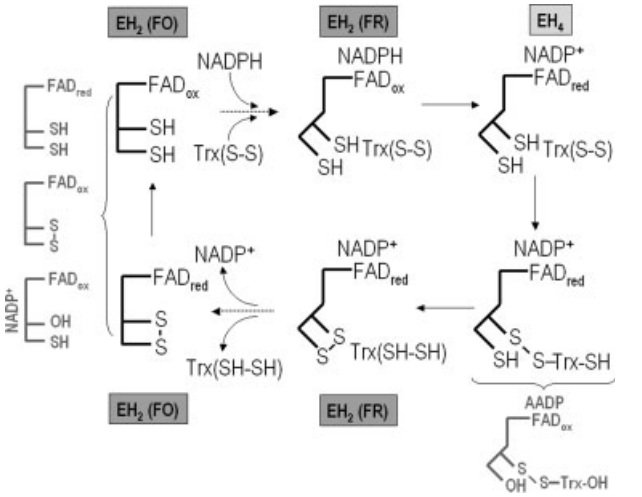

Figure 2

Schematic showing the different redox (EH_2 and EH_4) and conformational states (FO and FR) of TrxR during a full catalytic cycle (black lines and fonts) and in available X-ray crystal structures (grey lines and fonts). Serine and reduced cysteine residues are represented by —OH and —SH, respectively. Note that the nicotinamide group of NADPH can stack over the flavin ring of FAD only in the FR conformation.

Thus, for *E. coli* TrxR, little is still known about (i) the side-chain reorientations taking place along the path followed in the FO↔FR transition that moves the active-site dithiol from a buried position to the surface of the protein and the disulfide back onto the reduced flavin, (ii) the role that Trx itself plays in triggering this rotation and counter–rotation, (iii) the relative importance of residues involved in the binding and dissociation of both the Trx substrate and the NADP cofactor, and (iv) the structural characteristics of the catalytically competent intermediates.

To address these issues, we have employed a combination of computational modeling techniques, including normal mode analysis (NMA), protein–protein docking, molecular mechanics (MM), continuum electrostatics using both a generalized Born model (GB) and the Poisson-Boltzmann (PB) equation, solvent-accessible surface area (SA) calculations, and molecular dynamics (MD) simulations. This has allowed us to obtain a complete set of snapshots (describing the whole sequence of events leading from the binding of oxidized Trx to the release of reduced Trx) from which valuable information has been extracted and validated using several site-directed Trx mutants. We believe this study provides new insight into the catalytic mechanism of this enzyme, especially in relation to the intermediates that promote binding and dissociation of substrate and cofactor, and clarifies certain aspects that are not easily amenable to experimental techniques, particularly in relation to important transient interactions that are not currently visible in any of the structures experimentally determined to date.

MATERIALS AND METHODS

Quantum mechanical methods, molecular mechanics force field, and atom point charges

The geometries of FAD, $FADH_2$, $NADP^+$, and NADPH were first refined by means of the semiempirical quantum mechanical program MOPAC,[17] using the AM1 Hamiltonian and PRECISE stopping criteria, and further optimized using a restricted Hartree-Fock (RHF) method and a 6–31G(d) basis set, as implemented in the ab initio program Gaussian 03.[18] The resulting wavefunctions were used to calculate electrostatic potential-derived (ESP) charges employing the RESP methodology, as implemented in the AMBER suite of programs (http://amber.scripps.edu/). Dihedral parameters for the torsional barriers around the C—C bond linking the carboxamide group in NADPH and $NADP^+$ to the dihydropyridine/pyridinium ring were calculated so as to reproduce, in the AMBER force field using SPASMS,[19] the energy values calculated ab initio in Gaussian[18] (keyword SCAN) upon rotation of the bond every 15°. The remaining bonded and nonbonded parameters were assigned, by analogy or through interpolation from those already present in the AMBER database, in a way consistent with the second-generation AMBER force field[20] (parm99), which has been tested widely and used successfully in simulations of the type described herein.

Normal mode analysis

The X-ray crystal structures of TrxR (PDB entry 1TDF)[7] and the covalently trapped TrxR–Trx complex (PDB entry 1F6M)[9] at 2.0 and 2.95 Å resolution, respectively, were retrieved from the Protein Data Bank.[21] To probe the flexibility of this enzyme, an elastic network model was used in which all nonhydrogen protein atoms (within a cutoff of 10 Å) were modeled as point masses, and Cα atoms were connected by springs representing the interatomic force fields. The TrxR dimer from each PDB entry (with and without bound Trx), as well as one of the monomers, were analyzed as a large set of coupled harmonic oscillators using the NOMAD–Ref server[22] (http://lorentz.immstr.pasteur.fr/nomad-ref.php) and default parameters. The conformational changes were deduced by calculating the 10 lowest-frequency normal modes, which are those with the highest amplitudes and those most often related to large-scale structural rearrangements in proteins. Each mode was explored in its two opposite directions, thus resulting in two conformations different from the crystallographic structure within an rmsd value of 2 Å.

Model building, protein–protein docking and electrostatic calculations

The dimer structure of TrxR in the FO conformation[7,16] was generated from the monomer reported in the unit cell of PDB entry 1TDF by selecting the appropriate copy upon application of the crystallographic symmetry operators as implemented in the computer graphics program PyMOL[23] (http://pymol.sourceforge.net/). The protein–protein docking program ClusPro[24] (http://nrc.bu.edu/cluster/) was then employed to suggest feasible TrxR–Trx complexes using the Trx_{ox} crystal structure solved at 1.65 Å resolution (PDB entry 2TRX)[25] and both monomeric and dimeric TrxR as the binding partners.

The Adaptive Poisson-Boltzmann Solver (APBS)[26] implemented in PyMOL was used to calculate molecular electrostatic potentials (MEP). Cubic grids with a resolution of 1 Å were centered on the molecular systems considered following removal of the explicit water molecules, and the charges were distributed onto the grid points. Solvent-accessible surfaces, calculated with a spherical probe of 1.4 Å radius, defined the solute boundaries, and a minimum separation of 10 Å was left between any solute atom and the borders of the box. The potentials at the grid points delimiting the box were calculated ana-

lytically by treating each charge atom as a Debye–Hückel sphere. The protein interior was considered a low-dielectric medium ($\varepsilon = 4$), whereas the surrounding solvent was treated as a high-dielectric medium ($\varepsilon = 80$).

Target and reference structures for the FO→FR and FR→FO transition simulations

In the tMD study of the FO→FR transition the initial complex contained the TrxR(SH—SH)—FAD—Trx_{ox} assembly with TrxR as a monomer and the externally bound adenine dinucleotide as NADPH. Although, for computational efficiency, the TrxR monomer was used, Trx was docked as found in the best-scoring ClusPro solution obtained for the TrxR dimer, for reasons outlined below. The target structure was modeled using chains A and C of the covalently trapped TrxR—Trx complex (PDB entry 1F6M)[9] as a template followed by breaking of the mixed disulfide, replacement of Ser32 in Trx and Ser135 in TrxR by cysteines, creation of the Cys32-Cys35 disulfide bridge in Trx as found in PDB entry 2TRX,[25] modeling of Cys138 as a thiol, and replacement of AADP with NADPH. For the FR→FO transition, chains A, B, and C from PDB entry 1F6M[9] were used to model the initial structure in which TrxR appears as a dimer and the 3-aminopyridine ring of an AADP molecule stacks over the flavin of FAD. To build the required TrxR(S—S)—$FADH_2$—Trx_{red} complex FAD was reduced, the mixed disulfide was broken, Ser32 in Trx and Ser135 in TrxR were replaced by cysteines, a disulfide bridge was created between Cys135 and Cys138 of TrxR, Cys32 of Trx was modeled as a thiolate, and AADP was replaced with $NADP^+$. The corresponding target structure was modeled using as a template PDB entry 1TDF,[7] which contains TrxR in the FO state as a monomer, after generation of the appropriate symmetry-related copy in PyMOL to build the dimer, replacement of Ser138 with a cysteine and FAD with $FADH_2$, definition of a disulfide bridge between Cys138 and Cys135, and setting the active-site Cys32 and Cys35 of Trx as a thiolate and a thiol, respectively.

Molecular dynamics simulations

Both unrestricted (uMD) and targeted (tMD) molecular dynamics simulations were carried out using the AMBER 8.0 suite of programs.[19] Each molecular system was neutralized by the addition of sodium ions[27] and immersed either in a rectangular box of ~14,000 TIP3P water molecules[28] (for simulations of the monomer) or in a truncated octahedron of ~24,000 TIP3P water molecules (for simulations of the dimer) on which periodic boundary conditions were applied. Electrostatic interactions were treated using the smooth particle mesh Ewald method[29] with a grid spacing of 1 Å. The cutoff distance for the nonbonded interactions was 9 Å. The SHAKE algorithm[30] was applied to all bonds, and an integration step of 2.0 fs was used throughout. Solvent molecules and counterions were relaxed by energy minimization and then allowed to redistribute around the positionally restrained protein–protein complex (25 kcal mol^{-1} $Å^{-2}$) during a 50 ps run at constant temperature (300 K) and pressure (1 atm). These initial harmonic restraints were reduced gradually in a series of progressive energy minimizations until they were completely removed. The resulting systems were heated again from 100 to 300 K during 20 ps and allowed to equilibrate in the absence of any restraints for 1.0 ns during which system coordinates were collected every 2 ps for further analysis. These equilibrated structures were then used as the starting points for the tMD or uMD simulations each lasting either 1 or 10 ns, respectively.

The tMD approach[31,32] made use of the standard implementation incorporated into AMBER 8.0, which allows the solvent molecules to move freely and follow the dynamics of the protein. A restraint was defined in terms of a root-mean-square (rms) superposition to the final reference structure (target) and applied in the force field as an extra energy term of the following form:

$$E = 0.5k_r N(\text{rmsd} - \text{trmsd})^2 \quad (1)$$

where k_r is the force constant, N is the number of atoms, rmsd is the mass-weighted rms deviation of the initial structure (either FO or FR) with respect to the target structure (either FR or FO, respectively), and trmsd is the desired rms deviation value, which we set to zero. A force constant of 0.25 kcal mol^{-1} $Å^{-2}$ over 1.0 ns using in the rms definition all non-H atoms of both TrxR and Trx in the (NADPH:TrxR(SH—SH)—FAD)Trx(S—S) complex proved sufficient to find a low-energy path leading from the FO to the FR state (FO→FR transition). However, a force constant of 0.5 kcal mol^{-1} $Å^{-2}$ over 1.0 ns was applied in the case of the FR→FO transition for the ($NADP^+$:TrxR(S—S)—$FADH_2$)Trx(SH,S^-) complex using all atoms except Trx, $NADP^+$ and the TrxR side-chains in the rms definition. The rationale for this difference in the procedure is that in the first case the target structure has been determined experimentally, whereas in the second case Trx_{red} and $NADP^+$ must exit and they are allowed complete freedom during the simulation, just the same as the TrxR side-chains. Finally, and with the sole purpose of evaluating ClusPro's docking efficiency, a second "fake" FR→FO transition on the (NADPH:TrxR(SH—SH)—FAD)Trx(S—S) complex was simulated over 1.0 ns using a force constant of 0.25 kcal mol^{-1} $Å^{-2}$ applied only to non-H atoms of TrxR so that Trx could freely accommodate on the TrxR surface. This result was then compared with the best-scored ClusPro solution.

MM-GBSA BINDING CALCULATIONS

The binding free energy describing protein-ligand (e.g., TrxR–NADPH/$NADP^+$) or protein–protein (e.g., TrxR–

Trx) associations is the difference between the free energy, G, of the complex and that of the respective binding partners:

$$\Delta G_{\text{bind}} = G_{\text{TrxR-cofactor}} - (G_{\text{TrxR}} + G_{\text{cofactor}}) \quad (2a)$$

$$\Delta G_{\text{bind}} = G_{\text{TrxR-Trx}} - (G_{\text{TrxR}} + G_{\text{Trx}}) \quad (2b)$$

In these equations, the three G values usually denote averages over snapshots from independent MD trajectories of the molecular system at equilibrium. In our case, since the system is evolving along a reaction path connecting different conformational states, no averaging was done and each snapshot was analyzed individually:

$$\Delta G_{\text{bind}} = G_{\text{complex}}(i) - (G_{\text{protein}}(i) + G_{\text{ligand}}(i)) \quad (3)$$

where i denotes a snapshot taken from the tMD trajectory.

The value of G for each species was calculated using the following energy decomposition scheme, which is implemented in the MM–GBSA method within AMBER 8 (script mm_pbsa.pl)[33,34]:

$$\begin{aligned} G &= E_{\text{gas}} + G_{\text{sol}} - \text{TS} \\ E_{\text{gas}} &= E_{\text{int}} + E_{\text{ele}} + E_{\text{vdw}} \\ E_{\text{int}} &= E_{\text{bond}} + E_{\text{angle}} + E_{\text{torsion}} \\ G_{\text{sol}} &= G_{\text{GB}} + G_{\text{nonpolar}} \\ G_{\text{nonpolar}} &= \gamma\text{SASA} \end{aligned} \quad (4)$$

E_{gas} is the gas–phase energy, which is calculated using the AMBER force field[35,36] as the sum of internal energies (E_{int}), encompassing bond lengths (E_{bond}), bond angles (E_{angle}) and torsional angles (E_{torsion}), and coulombic (E_{ele}) and van der Waals (E_{vdw}) nonbonded energies. The solvation free energy, G_{sol}, is decomposed into polar and nonpolar contributions; the polar contribution (G_{GB}) is calculated by solving the generalized Born equation[37] using dielectric constants of 1 and 78.5 for solute and solvent, respectively, whereas the nonpolar contribution, G_{nonpolar}, is estimated from the solvent accessible surface area, SASA,[38] which is determined using a water probe with a radius of 1.4 Å. The surface tension constant γ was set to 0.005 kcal/mol/Å^2. T and S are the temperature and the total solute entropy, respectively. S is typically estimated on the basis of classical statistical formulae and NMA of representative snapshots of energy-minimized structures from a MD trajectory. In this investigation, this cumbersome procedure was obviated so that, in a first approximation, the solute entropy estimate was not included in the calculation of the free energy changes.

Alanine scanning mutagenesis

The MM-GBSA method was also used to perform "single-structure" computational alanine–scanning mutagenesis of Trx_{ox} during the FO→FR transition studied by tMD simulation. Arg73 and Lys36 residues were individually "mutated" to Gly and Ala, respectively. As before, the entropy term was not calculated because it was assumed, on the basis of previous work, that its contribution to ΔG_{bind} would be negligible.[39] On the other hand, the use of a single trajectory to calculate ΔG_{bind} is conducive to a much better agreement with the experimental data than when multiple trajectories are used.[40] It is then expected that, by using a single trajectory, error cancellation will overcome the insufficient sampling of the conformational space.[39,41]

Analysis of molecular dynamics trajectories

Three-dimensional structures and trajectories were inspected visually using the computer graphics program PyMOL.[23] Interatomic distances and angles, as well as root-mean-square deviations from a given structure, were monitored using the PTRAJ module in AMBER.[19]

Purification of WT and variant forms of *E. coli* thioredoxin

Plasmids pET 30a(+) encoding Trx were transformed into *E. coli* BL21 strain for protein overexpression. Cells were grown, starting from single colonies, at 37°C in LB medium with kanamycin. At an O.D._{600} of 0.6, protein overexpression was induced with isopropyl-beta-D-thiogalactopyranoside (IPTG). After 6 h, cultures were centrifuged, cell pellets were resuspended in 1 m*M* EDTA, 30 m*M* TRIZMA buffer, pH 8.3, and lysed using a French press. The cell debris was centrifuged, and the supernatant was collected and stirred with streptomycin sulfate (10% w/v) at 4°C overnight to precipitate nucleic acids. After centrifugation, the supernatant was loaded onto a 2 L Sephacryl S-100 high-resolution (Amersham Pharmacia Biotech) gel filtration column equilibrated in 1 m*M* EDTA, 30 m*M* TRIZMA buffer, pH 8.3. Trx fractions were identified by SDS-PAGE, pooled, and applied to a 250-mL Fractogel EMD DEAE (M) (Merck) ion exchange column equilibrated in 1 m*M* EDTA, 30 m*M* TRIZMA buffer, pH 8.3. The protein was eluted by a salt gradient (between 0 and 0.5 *M* NaCl). The proteins were pure as determined by SDS-PAGE.

Activity assays

The activities of wild-type (wt) Trx and several variants were determined by measuring the rate of insulin reduction spectrophotometrically at 650 nm as turbidity formation from the precipitation of the free insulin B chain.[42] Insulin solution (50 µL of 10 mg/mL) were

added to the activity buffer (potassium phosphate 0.1*M*, 2 m*M* EDTA). Different amounts of each mutant were added to the cuvette, and the reaction was started by addition of 10 μL dithiothreitol 0.1*M*, which causes Trx reduction. The activity was determined as the maximum value of the slope in a plot of absorbance at 650 nm versus time. Blank corrections were performed but were invariably small. For each Trx variant, several activity determinations were carried out at different protein concentrations. Specific activity values were derived from the linear dependence of activity with protein concentration.

Differential scanning calorimetry

A capillary VP-DSC calorimeter from MicroCal (Northhampton) was used. DSC experiments were performed in 5 m*M* HEPES buffer, pH 7, at a scan rate of 2.5 K/min. Calorimetric cells were kept under an excess pressure to avoid degassing during scan and to allow scans to proceed above 100°C without boiling. Additional details about the DSC experiments can be found in previous publications.[43,44] Reheating runs were performed routinely to check for reversibility.

RESULTS AND DISCUSSION

The reaction steps throughout a complete catalytic cycle of wild-type *E. coli* TrxR were studied herein by performing a series of tasks that are enumerated in Figure 1 and can be summarized as follows: (i) automated docking of Trx_{ox} onto TrxR in the FO conformation; (ii) exploration of normal modes on monomeric and dimeric TrxR, both in the presence and in the absence of bound Trx_{ox}; (iii) modeling and equilibration using unrestrained MD (uMD) of the TrxR-Trx_{ox} complex as found at the end of the reductive half-reaction, that is, with TrxR containing FAD and both Cys135 and Cys138 as thiols; (iv) simulation of the FO→FR transition for the preceding complex using targeted MD (tMD), so as to bring the active-site dithiol in close proximity to the active-site disulfide of Trx_{ox}, followed by relaxation of the same complex using uMD, with the aim of exploring the possible conformational rearrangements that are necessary for attack of TrxR Cys138 onto the Trx_{ox} disulfide; (v) building the TrxR-Trx mixed disulfide intermediate through bond connectivity reassignment, equilibration using uMD, and comparison with the TrxR(Cys135Ser)–Trx(Cys35Ser) X-ray crystal structure; (vi) topology remodeling and simulation using uMD of the TrxR-Trx complex at a step following resolution of the mixed disulfide by nucleophilic attack of TrxR Cys135, that is, with a reduced Trx (Trx_{red}) bound to TrxR in the FR conformation but with its active site Cys residues forming a disulfide; (vii) simulation of the FR→FO transition for the preceding complex using tMD so as to bring the active-site disulfide of TrxR adjacent to the flavin of $FADH_2$; and, finally, (viii) relaxation using uMD of the same complex to study the factors that favor Trx_{red} release and facilitate reduction of the disulfide bridge in TrxR so as to bring the system back to the first step of the catalytic cycle (as described in task 3).

Note that, for simplicity, NADPH binding and hydride transfer from NADPH to FAD are not explicitly included in the above summary but, from visual inspection of the individual structures resulting from the catalytic cycle (Fig. 1), it becomes clear that NADPH can externally bind to the enzyme only when TrxR is found in the FO state. Then, during the FO→FR transition, NADPH has to slide along its binding pocket so as to eventually place the reduced nicotinamide moiety adjacent to the isoalloxazine ring of FAD in a position suitable for hydride transfer. Likewise, $NADP^+$ must slide from the interior of the protein to the surface during the FR→FO transition, at the end of which it finally exits the enzyme, which is again found in the FO conformation.

The results produced by following this stepwise procedure facilitate our understanding of the intermediate states available for reduced and oxidized cofactor exchange and also thiol-disulfide exchange. The quantum mechanical (QM) aspects of the S_N2 reactions have not been addressed because they have been extensively and very accurately characterized by other authors using much simpler model systems.[45,46] A hybrid QM/MM[47] study of these reactions within the whole enzyme would be prohibitively expensive from a computational point of view and would not represent a significant advantage in terms of new knowledge over the results presented and discussed below.

Docking of Trx_{ox} onto TrxR in the FO conformation

Different solutions were found by the ClusPro program depending on whether the monomeric or dimeric form of TrxR was used in the calculations. For the monomer, the best-ranked solutions placed Trx_{ox} at the dimerization interface of TrxR. In a second cluster, Trx_{ox} appeared bound to the FAD-binding domain, and only in 1 out of 50 solutions was Trx_{ox} located close to the NADP-binding domain and with the active-site disulfide suitably oriented towards TrxR. On the other hand, when the TrxR dimer was used as the target the top-scoring solutions placed Trx in the right location and with the disulfide in an orientation suitable for catalysis. Most importantly, the positively charged side-chain of Arg73 of Trx pointed towards a pocket that is occupied by this same residue in the X-ray crystal structure of the covalently trapped complex between Trx(Cys35Ser) and TrxR(Cys135Ser) in the FR conformation (Fig. 3). This cavity, which is part of a groove on the surface of the

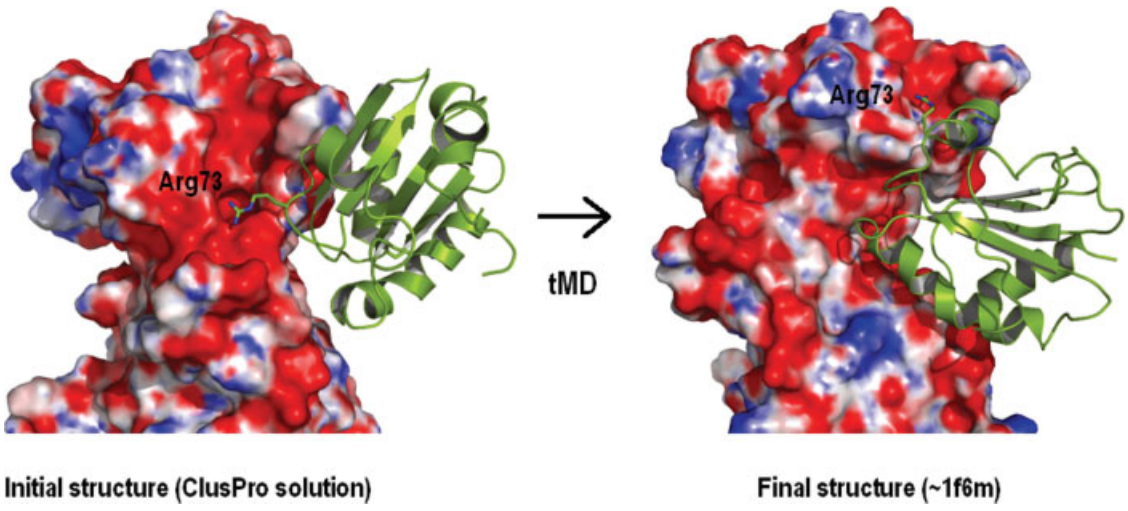

Figure 3

Close-up view of the NADP-binding domain of TrxR enveloped in a van der Waals surface that has been colored according to the molecular electrostatic potential (MEP) calculated by the APBS program (positive and negative regions in blue and red, respectively).[26] The green ribbon represents oxidized Trx, which is shown docked as suggested by the ClusPro program (left) and at the end of the tMD procedure (right) that brought TrxR from the initial FO state to the FR conformation. Note the negative character of the MEP both in the pocket where the guanidinium of Arg73 is lodged in the starting structure and in the groove that allows sliding of this residue during this conformational transition.

NADP-binding domain,[8] displays a highly negative molecular electrostatic potential (MEP) that mostly arises from the backbone carbonyl groups of Arg130, Gly131, Gln146, Val217, Ala237, and Leu239, as well as the side chain of Tyr143, in the FR conformation, and the backbone carbonyl groups of Glu48, Gly129, Arg130, Gly131, Val132, and Ser133, together with the side chains of Thr46, Glu48, Ser133, Asp139, and Tyr143 in the FO conformation. This result is strongly suggestive of the importance of Arg73 in Trx for productive binding to TrxR. Of note, this residue is highly conserved in bacterial Trx's, with the notable exception of *M. tuberculosis* Trx, in which the positionally equivalent amino acid is a valine. Interestingly, in low-molecular-weight TrxR's Tyr143 is also highly conserved, with the exception of *M. tuberculosis* TrxR, in which this position is occupied by a phenylalanine.

Normal mode analyses of TrxR

A single normal mode connecting FO and FR conformations was easily found in all cases, independently of whether TrxR was free or in complex with Trx. This mode faithfully reproduces the twisting motion that is used to interconvert these two conformational states in both directions (FO→FR and FR→FO) even though the amplitude of the movement of the NADPH-binding domain relative to the FAD-binding domain, under the default simulation conditions, was less than that observed by comparing FO and FR experimental structures (Fig. 4). Interestingly, when monomeric TrxR in the FO conformation was used as the starting point, this interconversion was described by the second nontrivial lowest frequency mode (upon removal of the six rigid motions of rotation and translation), in agreement with similar

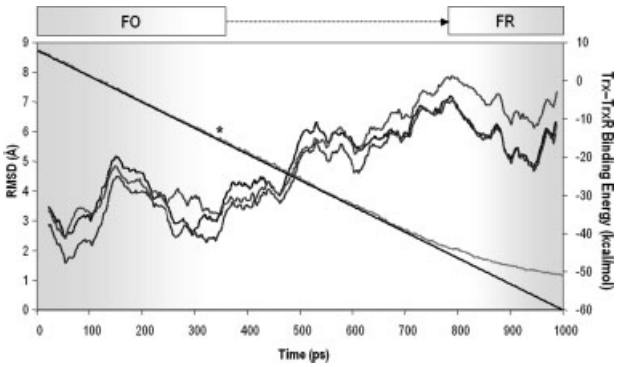

Figure 4

Left ordinate. Time evolution of the root-mean-square deviation (rmsd) between initial and target structures during the tMD simulation that connected FO and FR conformational states of TrxR. The diagonal straight line of negative slope represents the progressively decreasing target rmsd values. Actual simulation values are represented by the mostly overlapped grey line. The asterisk indicates the conformational state of *M. tuberculosis* TrxR in the crystal structure.[15] Right ordinate. Time evolution of the interaction energy between TrxR and either wild-type Trx (dark grey line) or mutant Trx (Lys36Ala, black line; Arg73Gly, light grey line). In all cases, the data were smoothed after filtering high-frequency noise by "moving window" averaging (boxcar smoothing) using a window of 11 sets of values. The progressively fading shaded area on both sides shows the regions that were explored in the normal mode analysis starting from either FO or FR states.

observations reported for *M. tuberculosis* TrxR.[15] This was also the case when the FR conformation was used in the absence of bound Trx. However, when the elastic network model was applied to Trx-bound TrxR in the FR conformation we found that the motion towards the FO state was dominated by the first nontrivial lowest frequency mode. We found an explanation for this apparent discrepancy when we studied the Trx_{ox}–TrxR complex that we modeled in the docking study reported above. In this case, the first nontrivial mode (mode 7) described a tighter fitting of Trx onto the TrxR surface that involved a relatively short displacement of Trx and a small twist of the NADPH-binding domain of TrxR relative to the FAD-binding domain whereas the second non-trivial mode (mode 8) effectively connected FO and FR conformational states. This result is in line with the reported use of NMA to optimize the fitting of two proteins.[48]

When the dimeric structure of TrxR in the FR conformation was studied, in the presence or in the absence of noncovalently bound Trx, the first and second nontrivial modes (modes 7 and 8), respectively, were also found to connect both conformational states. On the other hand, for the same dimer in the FO conformation the behavior in the presence of bound Trx was the same as that described above for the monomer, whereas in the absence of Trx it was mode 9 that described the interdomain twisting motion.

Interestingly, the reported crystallographic structure of *M. tuberculosis* TrxR in the FO state actually corresponds to an early intermediate state of *E. coli* TrxR in its transition from the FO conformation to the FR state, as studied by NMA (see the asterisk in Fig. 4).

NADPH can only bind to EH2 in the FO conformation (TrxR(SH)2–FAD–Trxox microstate)

The FO conformation of TrxR allows flavin oxidation by the disulfide (hence its name) or, in other words, reduction of the disulfide by $FADH_2$ (hence the name reductive half-reaction). This state is overtly the most stable as surmised from all the crystallographic evidence and, from the NMA reported earlier, it seems plausible that it is also the target for Trx_{ox} binding. This binding event would then trigger the internal motion that will bring the reduced active-site thiols to the outer surface of the enzyme in close proximity to the disulfide group of Trx_{ox}. Consistent with this, we modeled the complex of Trx_{ox} bound to TrxR in the FO conformation with an oxidized FAD molecule and both active-site Cys residues as thiols ($TrxR(SH)_2$–FAD–Trx_{ox} microstate). An externally bound NADPH molecule was also included because it has to be realized that the reduced cofactor can only bind to TrxR at this point in the catalytic cycle if it is to penetrate deeper into its binding pocket at a later stage to juxtapose its reduced nicotinamide ring over the oxidized isoalloxazine ring of FAD to eventually yield $FADH_2$. The nonproductive binding mode for NADPH reproduced that observed in the *E. coli* Trx_{ox}–TrxR complex[7] for $NADP^+$ but we found it necessary, for reasons outlined below, to rotate the carboxamide group attached to the pyridine ring by 180° so as to mimic the orientation reported in the X-ray crystal structure of *H. pylori* TrxR. Relaxation and equilibration of this system using energy minimization followed by uMD for 1 ns allowed slight reorientations of side-chains but did not lead to any significant conformational changes.

Simulation of the FO→FR transition

Test calculations for up to 10 ns showed that random thermal fluctuations within the system were not sufficient, as expected, to surmount the energy barrier separating FO and FR conformations in a reasonable simulation time. For this reason we used a tMD approach, as explained in the Methods section, to gradually force the TrxR–Trx system in the FO state to adopt the conformation found in the FR state over the course of a molecular dynamics trajectory.

Entry of NADPH

In the available crystal structures of prokaryotic TrxR's the NADP molecule always appears in the oxidized form and bound on the surface of the enzyme in a location that would be unsuitable for NADPH to transfer the hydride to FAD. It is then important to ascertain in which part of the catalytic cycle $NADP^+$ can be exchanged with its reduced counterpart. Since in the following FR→FO transition the active-site disulfide will be placed adjacent to the flavin, the only chance for the reduced nicotinamide ring of NADPH to approach the FAD prosthetic group is during the FO→FR transition. For this reason we modeled NADPH in the same location as that found for $NADP^+$ and simulated the twisting motion of TrxR (in the presence of bound Trx_{ox}) using tMD, as described below, so that the externally bound reduced cofactor could penetrate into the active site where the reductive half-reaction takes place and adopt a position equivalent to that experimentally found for the nonreducing analog AADP. Importantly, we only succeeded in doing so when the initial conformation of the nicotinamide was that described for *H. pylori* TrxR[14] instead of that reported for *E. coli*.[8] This is because optimal stacking between the nicotinamide and isoalloxazine rings occurs only when the nitrogen and oxygen of the carboxamide group of NADPH juxtapose O4 and N3 atoms, respectively, of the flavin rather than the reverse. On the other hand, the overall conformation of NADPH hardly changes as it slides from the enzyme's surface into the redox active site (Figure S1 of Supporting Information).

Dependence on the initial placement of Trx

When the tMD simulations on the TrxR–Trx–NADPH complex started from the ClusPro solution calculated for the monomeric form of TrxR that docked Trx in the NADPH-binding domain, the final structure did not perfectly match the target. Even though the root-mean-square (rms) deviation for backbone atoms systematically decreased and the initial structure approached very closely the desired conformation (rmsd = 0.74 Å) the side chain of Arg130 in TrxR, rather than establishing a hydrogen bond with the carbonyl oxygen of Tyr70 in Trx, as found in the target structure, stacked on the indole ring of Trp31 of Trx half-way through the simulation (data not shown). In this location, this Arg130 systematically prevented lodging of the side chain of Arg73 of Trx into its binding pocket in TrxR, regardless of simulation conditions.

Only when the best-scored ClusPro solution calculated for the dimeric form of TrxR was used did we succeed in decreasing the rmsd for the backbone still further (0.68 Å) and achieving a final structure that was perfectly superimposable to that of the target conformation. This finding validates the tMD approach as a useful technique in the study of this type of molecular associations but also highlights the fact that sometimes small subtleties at the protein–protein interface that can pass relatively unnoticed may have a great influence on subsequent attempts to optimize the fitting between the two structures. In addition to the important electrostatic interactions involving Arg73, the driving of Trx to the final docked conformation appears to be guided by important hydrophobic contacts that are progressively gained between Trp31 (Trx) and Phe141 (TrxR), Met37 (Trx) and Phe81 (TrxR), and Gly74 (Trx) and Phe142 (TrxR), all of which can be seen in the experimental structure of the covalently trapped TrxR–Trx complex.[9] On the other hand, another possibly important interaction is that transiently observed between Lys36 (Trx) and Glu66 (TrxR), which is present in our initial complex originating from the docking study but does not appear in the experimentally determined TrxR–Trx complex.

Interestingly, when the conformational change was simulated in the opposite direction (FR→FO, for the sake of comparison only), the final location of Trx was almost identical (rmsd = 1.07 Å for all nonhydrogen atoms) to that found by ClusPro for the dimeric enzyme, even when no extra force was applied to any Trx atoms during the tMD simulation (Methods section for details). This result also validates the tMD approach and additionally provides some indirect evidence in support of the proposal that this is the binding mode of this substrate to TrxR.

It is important to realize that the reaction intermediates that make NADPH entry possible are the same or structurally very close to those showing binding of Trx_{ox} to TrxR, as these two events must occur almost simultaneously for the reaction to proceed. In other words, substrate and cofactor binding are coupled during the same twisting motion. An important aftermath is that, as the nascent dithiol is generated and has to be relocated on the surface of the enzyme, the presence of bound Trx_{ox} largely shields the reactive thiol of Cys138 from the solvent, thus avoiding its unspecific premature oxidation (Figure S2 of Supporting Information).

Binding energy analysis and experimental validation

In our simulations, the binding of NADPH, in common with the binding of $NADP^+$ as observed in the X-ray crystal structures of TrxR in which this molecule has been solved, is dominated by electrostatic interactions between the cofactor phosphates and a cluster of arginine residues (Arg117, Arg176, Arg177, Arg181, and Arg293). These interactions are maintained during the twisting motion that connects FO and FR states and constitute the main driving force that directs the reduced nicotinamide ring towards the oxidized flavin. It is only at the end of the FO→FR simulation, when the nicotinamide and isoalloxazine ring systems stack, that the interaction energy between the cofactor and the enzyme (plus the prosthetic group) is improved (Fig. 5). These results will be compared later with those obtained for the exit of $NADP^+$ during the reverse FR→FO simulation.

When the MM-GBSA approach was used to get an estimation of the changes in intermolecular binding energy taking place during the FO→FR transition (Fig. 4), we observed that the most favorable TrxR–Trx binding energy corresponds to the phase space in the vicinity of the FO conformation and the least favorable one to those structures in which TrxR is close to the FR state. In fact, the energy maximum detected at ~800 ps corre-

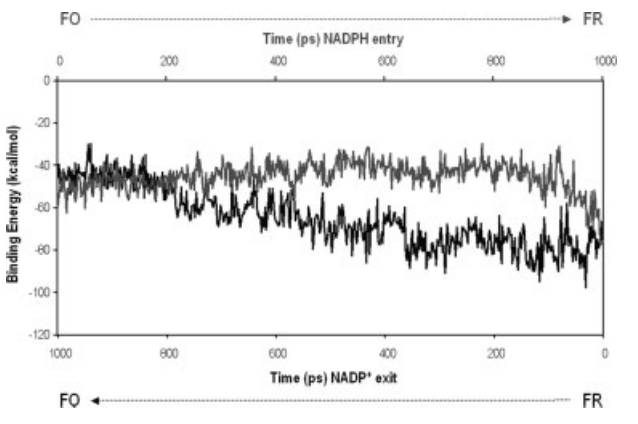

Figure 5

Time evolution of the interaction energy between the cofactor and the enzyme (plus the prosthetic group) during the FO→FR simulation (NADPH entry) and the reverse FR→FO simulation ($NADP^+$ exit). Note that the interaction energy favors binding of NADPH over $NADP^+$ when TrxR is in the FO state and also that the energy values for both redox states of the cofactor at the FR end-point, where hydride transfer from NADPH to FAD takes place, are remarkably similar.

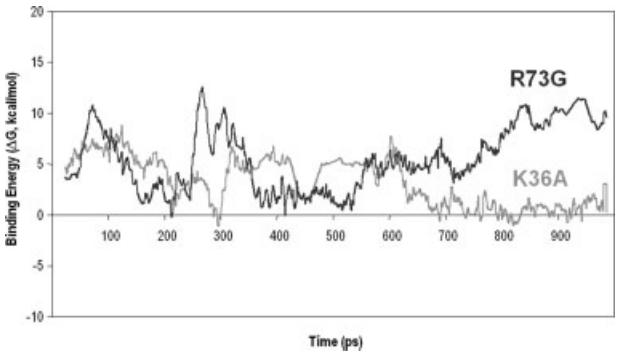

Figure 6

Plot of the differences in TrxR–Trx binding energies for Lys36Ala (black line) and Arg73Gly (grey line) mutant thioredoxins relative to wild-type during the FO→FR transition. Note that the loss of binding energy is much more pronounced and persistent for the Arg73Gly mutant than for the Lys36Ala mutant.

sponds to the structure in which the distance between the attacking thiol of Cys138 and the sulfur atom of Cys32 that makes up the disulfide with Cys35 in Trx_{ox} reaches a plateau at ~5 Å (Figure S3 of Supporting Information). It is also at this point that the Cys138 thiol is virtually occluded from the solvent by Trx, as discussed above and shown in Figure S2 of Supporting Information, and also when both carboxylate oxygens of Asp139 are positioned at such short distance of the Cys138 thiol (Figure S3 of Supporting Information) that they could possibly abstract the proton to yield the thiolate that will eventually perform the nucleophilic attack on the disulfide. An attack by a thiolate in preference to a thiol would be in agreement with high-level quantum mechanical calculations.[45] In this respect, it is of interest that an Asp139Asn mutant TrxR showed only about 1% of the activity of the wild-type enzyme in the oxidative half-reaction, and an Asp139Leu mutant was completely inactive.[49] Therefore, our simulations provide additional support to the view that Asp139 of TrxR behaves as the acid-base catalyst that was invoked to account for the pH dependence of the redox potential of TrxR.

Following this energy maximum, the complex relaxes and the intermolecular interaction improves until, near the end of the tMD simulation, the enforced intermolecular S—S distance makes the energy rise again due to electrostatic and van der Waals repulsion between the nonbonded sulfur atoms, which are being brought as close as they are found in the target structure corresponding to the mixed disulfide. Nonetheless, it must be born in mind that at this point both the S—S distance and the angle of attack of the thiol (or the thiolate if Cys138 is deprotonated by Asp139) on the disulfide (Figure S3 of Supporting Information) are the most favorable for the S_N2 reaction to proceed.[45]

To gain insight into the importance of the contribution of selected residues to the intermolecular binding energy, we focused on Arg73 and Lys36 of Trx. During the simulations Arg73 was seen to interact with its malleable binding groove in TrxR from beginning to end and its position was found to be crucial in the protein docking experiments, as discussed earlier. On the other hand, a close electrostatic interaction between Lys36 of Trx and Glu66 of TrxR is present in our model of the complex with TrxR in the FO conformation but not in that representing the FR state. The relative importance of these two Trx residues was assessed by carrying out a series of MM-GBSA calculations on the same set of snapshots from the tMD trajectory but after replacement of the residue of interest with either Ala (computational alanine-scanning mutagenesis) or Gly. The results for the Lys36Ala and Arg73Gly mutants (Fig. 6) strongly suggest that both residues contribute significantly to the binding energy during the twisting motion that connects FO and FR states and also that Lys36 interacts with TrxR in a more transient manner than does Arg73. Thus, our simulations support the presumed importance of Arg73 as a crucial residue for Trx binding[9] and additionally highlight the possibility that Lys36 is involved in transient interactions that are observed in some snapshots from the trajectory but are absent in the only TrxR–Trx experimental structure currently available.

Consistent with these computational results, when we measured the ability of Lys36Ala and Arg73Gly Trx mutants to be used as substrates for TrxR in comparison with wt-Trx, we found that the Arg73Gly mutant could hardly be reduced by this enzyme, whereas the Lys36Ala mutant was compromised in this ability to a lesser extent (Fig. 7). Furthermore, an Arg→Asp substitution at posi-

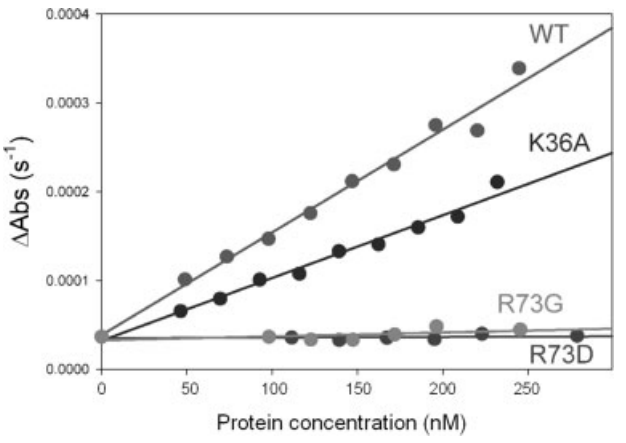

Figure 7

Activity of TrxR on wild-type and mutant thioredoxins. Catalytic rates were 1156.9, 705.9, 43.4, and 7.1 ΔAbs s^{-1} M^{-1} for wt, K36A, R73G, and R73D, respectively. Note that the deleterious effect of removing the side-chain of Arg73 is further increased when a negatively charged side-chain is incorporated at this position.

tion 73, which involves a reversal in the electrostatic character of the side chain, was even more deleterious because TrxR was virtually unable to reduce this Arg73Asp Trx mutant. These decreased activities were not the result of Trx denaturation as the thermostabilities of wt-Trx and the mutant proteins were very similar (as judged by changes in melting temperatures $\leq$ 1.5 K) and all of them behaved similarly in the insulin turbidimetric assay (Figure S4 of Supporting Information), that is, they were as competent as the wild-type protein in transferring reducing equivalents to a typical Trx substrate.[43] Consequently, we believe that the observed reduced activities result from the impaired binding of the mutant Trx's to TrxR predicted by our calculations. In fact, upon completion of this work, we realized that a Lys36Glu mutant Trx had been studied previously using stopped-flow techniques.[50] This mutation was shown not to have a major impact on the structure of the protein but resulted in less tight binding to TrxR at low ionic strengths, a decrease in V_{max}, and a clear dependence of the reaction rate of TrxR on substrate concentration, which is not seen with wt-Trx. Our data now provide a structural rationale to these findings and point to Glu66 as the residue in TrxR most likely to establish a direct electrostatic interaction with Lys36 in Trx.

Formation, equilibration and breakdown of the TrxR–Trx mixed disulfide intermediate

Near the end of the simulation of the FO→FR transition, both the S—S distance separating Cys138 in TrxR and Cys32 in Trx and the S—S—S angle of attack were close to the optimal values (less than 5 Å and near 180°) calculated theoretically[45] for the first S_N2 reaction leading to the mixed disulfide (Figure S3 of Supporting Information). Concomitant with the disulfide-thiol interchange event taking place at the protein-protein interface, reducing equivalents are being transferred from NADPH to FAD in the enzyme interior to yield $NADP^+$ and $FADH_2$. It is at this point in the catalytic cycle, therefore, that the EH_4 intermediate is generated, as depicted in Figures 1 and 2.

Formation and equilibration of the mixed disulfide intermediate

By changing the connectivity of the sulfur atoms involved in the first S_N2 reaction (rightmost schemes in Fig. 2) we generated a new topology[51] for the TrxR-Trx complex that enabled us to relax the new geometry and then simulate the mixed disulfide complex using uMD. During the equilibration, comparison with the covalently trapped TrxR(Cys135Ser)–Trx(Cys35Ser) complex solved by X-ray crystallography[9] did not reveal any major conformational changes and highlighted the importance of a hydrogen-bonding network involving Ser133, Ala134, Cys135, Thr137, Asp139, Gly140, and Glu160 in the stabilization of the active-site geometry that is necessary for the second S_N2 reaction to proceed.

Breakdown of the mixed disulfide intermediate

We next studied the structural requirements that facilitate the breakdown of the TrxR–Trx mixed disulfide intermediate that will yield Trx_{red} and an oxidized TrxR. This is the second thiol-disulfide interchange reaction in the catalytic cycle, and it is effected by an S_N2 attack of Cys135 of TrxR onto the sulfur atom of Cys32 of Trx. In this regard, our simulation results suggest the plausibility of an increase in the reactivity of Cys135 due to deprotonation by Glu160 of TrxR to yield a thiolate, given the similarities in geometries with respect to the proposed Asp139-mediated deprotonation of Cys138 reported above (data not shown). In this case, however, to the best of our knowledge, experimental evidence supporting this role for Glu160 is lacking although we note that a glutamic acid at this position is strictly conserved in low-molecular-weight TrxR's.

Creation of the Cys135−Cys138 disulfide bond in TrxR entails breaking of the mixed disulfide and definition of a new topology in the system, which now consists of Trx_{red} bound to TrxR in the FR conformation but with its active-site cysteines forming a disulfide. In addition, it is also at this point that the hydride is transferred to FAD from NADPH so that reduced and oxidized forms of these two molecules need to be interchanged at a later stage. When we tried to equilibrate the resulting TrxR(S—S)—$FADH_2$—Trx_{red} microstate (EH_2 in the FR conformation) with bound $NADP^+$ using uMD, the trajectory was unstable because the isoalloxazine ring of $FADH_2$ failed to maintain a good stacking interaction with the nicotinamide moiety. This instability was notably accentuated during the subsequent tMD simulation. Reinspection of the crystal structure of the covalently trapped complex allowed us to notice that two important residues from the other subunit making up the TrxR dimer were missing in our simulated monomeric FR state: Tyr23, which is seen to interact directly with the flavin,[9] and Arg26, which participates in a hydrogen bonding network. Having realized the importance of considering the dimeric structure of the enzyme for a more accurate simulation of this part of the catalytic cycle, the equilibration of the TrxR(S—S)—$FADH_2$—Trx_{red} microstate and the subsequent FR → FO transition were carried out on a solvated system consisting of a single Trx bound to a dimeric TrxR.

During the equilibration of this macromolecular assembly using uMD the phenol group of Tyr23 kept engaged in a good hydrogen bond with the O2 of the flavin, thus providing additional stabilization to the bound prosthetic group, which now remained firmly in place. On the other hand, Arg26 was seen to play a major role in orienting and stabilizing the carboxylate of Glu183,

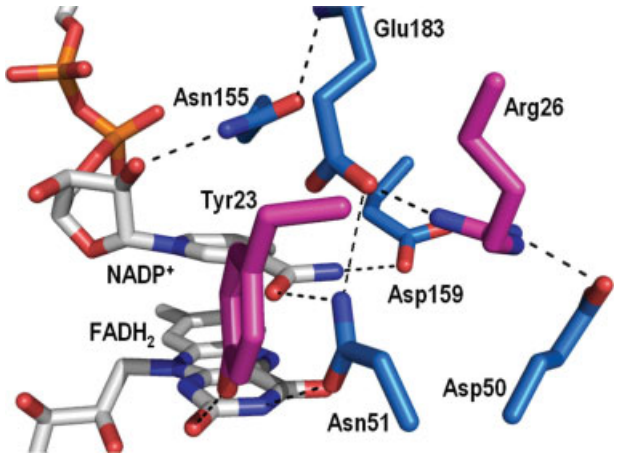

Figure 8

Close-up view of the cofactor binding site at the TrxR dimer interface showing the residues (carbon atoms in blue) mostly involved in the interaction network that helps fixate the $NADP^+$ molecule properly in place and stacked on the FAD prosthetic group (both ligands are shown with carbon atoms colored in white). Tyr23 and Arg26 (carbon atoms in magenta) belong to the other subunit making up the dimer.

which in turn fixates the side-chain of Asn51 in such a way that its carboxamide oxygen can hydrogen bond to N3 of $FADH_2$ (as seen in the crystal structure) and its NH_2 can establish a good hydrogen bond with the carbonyl group of the nicotinamide ring of $NADP^+$. In this orientation, the carboxamide of Asn155 (which is hydrogen bonded to the backbone NH of Glu183 and the ribose O2' of $NADP^+$) stacks in an antiparallel (and therefore electrostatically favorable) orientation on the carboxamide group of nicotinamide and the NH_2 group is also able to hydrogen bond to the carboxylate of Glu159, thus providing further support to our favored orientation of the cofactor in its binding site (Fig. 8). At this point, it is important to stress that these latter interactions have not been reported previously because the only experimental structure currently available for the FR state lacks the natural cofactor of the reaction given that the nonreducing AADP analogue was used instead.

Simulation of the FR→FO transition

Once the mixed disulfide was resolved, we ended up with a molecular system containing TrxR with an active-site disulfide, $FADH_2$, $NADP^+$, and a reduced Trx with Cys35 as a thiol and Cys32 as a thiolate, in agreement with the low experimental pK_a value determined for this cysteine[52] and previous theoretical work.[45,46,53]

To close the catalytic cycle shown in Figure 1 all that remained was to simulate the FR→FO transition for the dimeric TrxR in the preceding complex, again using tMD, so as to bring the active-site disulfide back to a position adjacent to the flavin of $FADH_2$, and relax the resulting structure using uMD. Of note, during this motion the oxidized cofactor must be exchanged for a new NADPH molecule and the reduced substrate must disassociate from the enzyme.

Exchange of $NADP^+$ and NADPH at the NADP-binding domain

During this transition the $NADP^+$ molecule, whose phosphates are bound on the enzyme surface while its nicotinamide ring is buried in the protein interior, must leave the enzyme. Since the only difference between the outgoing $NADP^+$ and the incoming NADPH is the presence of a positive charge on the oxidized nicotinamide moiety, we reasoned that, in addition to the twisting motion promoting the loss of the hydrogen-bonding interactions described above, there should be an important electrostatic component in the mechanism driving the exit of $NADP^+$. In fact, as soon as the hydride is transferred from NADPH to FAD and the pyridinium is generated, this positive charge alters the existing balance of interactions among the side-chains of Arg26 (from the other monomer), Asp50, Asp159 and Glu183 (Fig. 8). Electrostatic repulsion from Arg26 and attraction to the carboxylates act in unison with the interdomain twisting motion of TrxR to favor $NADP^+$ exit. Furthermore, visual inspection of the trajectory (Movie 1 of Supporting Information) allowed us to identify Arg293 as the residue that is most likely responsible for the final ejection of the positively charged oxidized cofactor because the distance separating the pyridinium ring of $NADP^+$ and the guanidinium of Arg293 became progressively shorter during the tMD simulation (Figure S5 of Supporting Information). In line with this reasoning, when we calculated the interaction energy between the oxidized cofactor and the whole of the TrxR enzyme using the MM-GBSA method we found a pattern that was reversed with respect to that previously found for NADPH binding and entry (Fig. 5). The rightmost part of this figure corresponds to the moment when NADPH transfers the hydride to FAD to yield $NADP^+$ (FR state of TrxR). The leftmost part of the figure corresponds to the moment when NADPH and $NADP^+$ can exchange (FO state of TrxR, as seen in the crystal structure, and represented at the top of Fig. 1), and it is at this point that the interaction energy appears to be more favorable for the reduced cofactor. During the ensuing equilibration using uMD of this TrxR(S—S)—$FADH_2$ microstate (EH_2 in the FO conformation) the repulsion energy kept increasing and the nicotinamide moiety became progressively more exposed to the solvent (data not shown). A second residue that might be important for pyridine nucleotide exchange is Tyr262, which gives rise to another transient interaction between its phenolic oxygen and the ribose O1' atom during this transition (Figure S5 of Supporting Information).

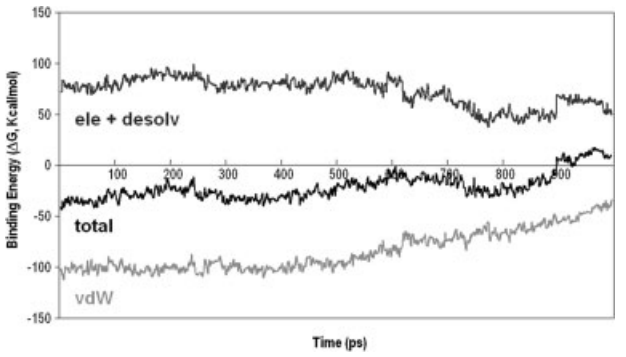

Figure 9

Time evolution of van der Waals (light grey), electrostatic + desolvation (dark grey) and overall interaction energy (black) between Trx_{red} and TrxR during the FR→FO transition.

Disassociation of reduced Trx from TrxR

The enzyme-substrate dissociation process became apparent from inspection of the binding free energy plot calculated using the MM-GBSA method. A progressive loss of van der Waals interaction energy between TrxR and Trx_{red} was detected half-way through the FR→FO transition, and it was consistently maintained until the end of the simulation (Fig. 9). The electrostatic energy term, on the other hand, also started to change mostly as a consequence of increased solvation of the binding partners but the overall free energy change remained favorable until 100 ps before the end of the simulation. At this point, when TrxR is already sampling the FO conformation, a peak is found due to decreased electrostatic attraction between Trx and TrxR that leads to an unfavorable overall binding free energy that is maintained during the ensuing equilibration using uMD (data not shown) and can account for the eventual dissociation of the two proteins. Interestingly, this decreased electrostatic interaction is accompanied by the loss of specific hydrogen bonds that were present in the transient intermediates connecting both conformational states. The most important ones (and in sequential order) are those between the positively charged amino group of Lys36 (Trx) and the carboxylate of Glu66 (TrxR), the backbone oxygen of Trp31 (Trx) and the hydroxyl of Thr60 (TrxR), and finally the side-chain of Arg73 of Trx and its binding cleft in TrxR. Thus, it can be seen that the same residues that promote formation of a productive complex are involved in the reverse process of dissociation.

CONCLUSIONS

By following the catalytic cycle of TrxR acting on Trx step by step using MD simulations, we have been able to structurally characterize a series of intermediates that cannot easily be individualized by experimental techniques. In our hands, this same approach proved its value before in the study of inhibitor entry into the allosteric site of HIV-1 reverse transcriptase,[32] the creation of an intercalation site in DNA,[54] and the stepwise dissection of the reaction carried out on several substrates by the dehalogenase enzyme LinB.[51] The TrxR–Trx complex studied herein is considerably more challenging insofar as it is a bulkier molecular system that is subjected to large conformational changes and comprises not only two proteins but also a prosthetic group and a cofactor, both of which can be found in either a reduced or an oxidized state. The tMD simulations allowed us to study in atomic detail the motions of rotation and counter-rotation that alternatively place either the nicotinamide ring of NADPH or the active-site disulfide adjacent to the flavin buried within TrxR and simultaneously allow the reduced active-site thiols/thiol-thiolate to move from a buried position to the enzyme surface where they can react with the Trx disulfide.

The binding mode we found for Trx_{ox} on TrxR and the results from ensuing MD simulations of the complex strongly suggested that Arg73 in Trx is a crucial residue for the initial electrostatic-driven binding of the two proteins and the subsequent twisting motion. Likewise, Lys36 was seen to give rise to a transient electrostatic interaction that is not observed in any of the experimental structures determined to date. The importance of these two residues was then probed by site-directed mutagenesis. Consistent with our expectations, Arg73Asp and Arg73Gly Trx mutants were found to be greatly impaired in their capacity to be reduced by *E. coli* TrxR, whereas a Lys36Ala mutant could still be reduced although less efficiently than wild-type Trx (the catalytic rate was decreased by half). Noteworthy, none of the mutants showed an appreciable change in thermostability, attesting to the lack of major structural effects, and all of them were competent as reducing agents in a standard assay in which Trx catalyzes the reduction of insulin by dithiothreitol.

Our simulations also provide a plausible explanation to the earlier finding that an Asp139Asn mutant TrxR displayed only about 1% of the activity of the wild-type enzyme in the oxidative half-reaction[49] as they show that the carboxylate of this aspartic acid can deprotonate the thiol of Cys138, thereby activating this residue for attack on the disulfide bond in the active site of Trx_{ox}. Along the same lines, our simulation results support the view that the reactivity of the Cys135 thiol in TrxR could also be increased due to deprotonation by Glu160 to yield a thiolate anion.

NADPH entry, which immediately precedes or is coupled to Trx_{ox} binding, and $NADP^+$ exit, which is coupled to or immediately follows Trx_{red} release, take place when TrxR is found in the FO conformation. Pyridine nucleotide exchange is eventually triggered by a re-

pulsive interaction involving Arg293 and the positively charged pyridinium moiety of $NADP^+$. This sort of interaction was not unexpected because the rest of the cofactor structure, which is anchored to the enzyme by means of the same amino acids, is identical in oxidized and reduced states. The only moment during the catalytic cycle that allows the generation of the biochemically characterized EH_4 microstate is before reduction of the Trx disulfide on the enzyme's outer surface (that is, before oxidation of the TrxR active-site dithiol) and after reduction of FAD in the enzyme interior by NADPH. This means that the EH_4 only exists in the FR conformation and cannot be represented by the artificially dithionite-reduced TrxR reported in currently available crystal structures.

On the basis of previous findings and the results reported herein, *E. coli* TrxR appears as a highly sophisticated and beautifully engineered molecular machine that is capable of synchronizing cofactor capture and ejection with substrate binding and redox activity.

ACKNOWLEDGMENTS

The authors thank Dr. Antonio Morreale (Centro de Biología Molecular Severo Ochoa, CSIC, Madrid) for his help in setting up the MM-GBSA calculations and for many fruitful discussions. They also thank Marta Camacho and Juan A. Bueren for help in the preparation of the artwork. The University of Alcalá Computing Center and the CIEMAT (Madrid) are gratefully acknowledged for generous allowances of computer time on their SGI servers.

REFERENCES

1. Williams CH, Jr. Mechanism and structure of thioredoxin reductase from *Escherichia coli*. FASEB J 1995;9:1267–1276.
2. Argyrou A, Blanchard JS. Flavoprotein disulfide reductases: advances in chemistry and function. Prog Nucleic Acid Res Mol Biol 2004;78:89–142.
3. Karplus PA, Schulz GE. Substrate binding and catalysis by glutathione reductase as derived from refined enzyme: substrate crystal structures at 2 Å resolution. J Mol Biol 1989;210:163–180.
4. Sandalova T, Zhong L, Lindqvist Y, Holmgren A, Schneider G. Three-dimensional structure of a mammalian thioredoxin reductase: implications for mechanism and evolution of a selenocysteine-dependent enzyme. Proc Natl Acad Sci USA 2001;98:9533–9538.
5. Berkholz DS, Faber HR, Savvides SN, Karplus PA. Catalytic cycle of human glutathione reductase near 1 Å resolution. J Mol Biol 2008;382:371–384.
6. Marcus RA, Sutin N. Electron transfers in chemistry and biology. Biochim Biophys Acta 1985;811:265–322.
7. Kuriyan J, Krishna TS, Wong L, Guenther B, Pahler A, Williams CH, Jr, Model P. Convergent evolution of similar function in two structurally divergent enzymes. Nature 1991;352:172–174.
8. Waksman C, Krishna TSR, Williams CH, Jr, Kuriyan J. Crystal structure of *Escherichia coli* thioredoxin reductase refined at 2 Å resolution. Implications for a large conformational change during catalysis. J Mol Biol 1994;236:800–816.
9. Lennon BW, Williams CH, Jr, Ludwig ML. Twists in catalysis: alternating conformations of *Escherichia coli* thioredoxin reductase. Science 2000;289:1190–1194.
10. Lennon BW, Williams CH, Jr. Enzyme-monitored turnover of *Escherichia coli* thioredoxin reductase: insights for catalysis. Biochemistry 1996;35:4704–4712.
11. Lennon BW, Williams CH, Jr, Ludwig ML. Crystal structure of reduced thioredoxin reductase from *Escherichia coli*: structural flexibility in the isoalloxazine ring of the flavin adenine dinucleotide cofactor. Protein Sci 1999;8:2366–2379.
12. Zheng YJ, Ornstein RL. A theoretical study of the structures of flavin in different oxidation and protonation states. J Am Chem Soc 1996;118:9402–9408.
13. O'Donnell ME, Williams CH, Jr. Proton stoichiometry in the reduction of the FAD and disulfide of *Escherichia coli* thioredoxin reductase. Evidence for a base at the active site. J Biol Chem 1983;258:13795–137805.
14. Gustafsson TN, Sandalova T, Lu J, Holmgren A, Schneider G. High-resolution structures of oxidized and reduced thioredoxin reductase from *Helicobacter pylori*. Acta Crystallogr D Biol Crystallogr 2007;63:833–843.
15. Akif M, Suhre K, Verma C, Mande SC. Conformational flexibility of *Mycobacterium tuberculosis* thioredoxin reductase: crystal structure and normal-mode analysis. Acta Crystallogr D Biol Crystallogr 2005;61:1603–1611.
16. Williams CH, Jr, Arscott LD, Muller S, Lennon BW, Ludwig ML, Wang PF, Veine DM, Becker K, Schirmer RH. Thioredoxin reductase. Two modes of catalysis have evolved. Eur J Biochem 2000;267:6110–6117.
17. Stewart JJP. MOPAC: a semiempirical molecular-orbital program. J Comput Aided Mol Des 1990;4:1–45.
18. Gaussian 03, Revision B.04, Frisch MJ, Trucks GW, Schlegel HB, Scuseria GE, Robb MA, Cheeseman JR, Montgomery JA, Jr, Vreven T, Kudin KN, Burant JC, Millam JM, Iyengar SS, Tomasi J, Barone V, Mennucci B, Cossi M, Scalmani G, Rega N, Petersson GA, Nakatsuji H, Hada M, Ehara M, Toyota K, Fukuda R, Hasegawa J, Ishida M, Nakajima T, Honda Y, Kitao O, Nakai H, Klene M, Li X, Knox JE, Hratchian HP, Cross JB, Bakken V, Adamo C, Jaramillo J, Gomperts R, Stratmann RE, Yazyev O, Austin AJ, Cammi R, Pomelli C, Ochterski JW, Ayala PY, Morokuma K, Voth GA, Salvador P, Dannenberg JJ, Zakrzewski VG, Dapprich S, Daniels AD, Strain MC, Farkas O, Malick DK, Rabuck AD, Raghavachari K, Foresman JB, Ortiz JV, Cui Q, Baboul AG, Clifford S, Cioslowski J, Stefanov BB, Liu G, Liashenko A, Piskorz P, Komaromi I, Martin RL, Fox DJ, Keith T, Al-Laham MA, Peng CY, Nanayakkara A, Challacombe M, Gill PMW, Johnson B, Chen W, Wong MW, Gonzalez C, and Pople JA. Gaussian, Inc.: Wallingford, CT; 2004.
19. Case DA, Cheatham TE, III, Darden T, Gohlke H, Luo R, Merz KM, Jr, Onufriev A, Simmerling C, Wang B, Woods RJ. The AMBER biomolecular simulation programs. J Comput Chem 2005;26:1668–1688.
20. Cornell WD, Cieplak P, Bayly CI, Gould IR, Merz KM, Ferguson DM, Spellmeyer DC, Fox T, Caldwell JW, Kollman PA. A second generation force field for the simulation of proteins, nucleic acids, and organic molecules. J Am Chem Soc 1995;117:5179–5197.
21. Berman HM, Battistuz T, Bhat TN, Bluhm WF, Bourne PE, Burkhardt K, Feng Z, Gilliland GL, Iype L, Jain S, Fagan P, Marvin J, Padilla D, Ravichandran V, Schneider B, Thanki N, Weissig H, Westbrook JD, Zardecki C. The Protein Data Bank. Acta Crystallogr D Biol Crystallogr 2002;58:899–907.
22. Lindahl E, Azuara C, Koehl P, Delarue M. NOMAD-Ref: visualization, deformation and refinement of macromolecular structures based on all-atom normal mode analysis. Nucleic Acids Res 2006;34Web Server issue:W52–56.
23. De Lano W. PyMOL version 0.99. DeLano Scientific LLC; 2006.
24. Comeau SR, Gatchell DW, Vajda S, Camacho CJ. ClusPro: a fully automated algorithm for protein-protein docking. Nucleic Acids Res 2004;32Web Server issue:W96–W99.
25. Katti SK, LeMaster DM, Eklund H. Crystal structure of thioredoxin from *Escherichia coli* at 1.68 Å resolution. J Mol Biol 1990;212:167–184.

26. Baker NA, Sept D, Joseph S, Holst MJ, McCammon JA. Electrostatics of nanosystems: application to microtubules and the ribosome. Proc Natl Acad Sci USA 2001;98:10037–10041.
27. Aqvist J. Ion water interaction potential-derived from free energy perturbation simulations. J Phys Chem 1990;94:8021–8024.
28. Jorgensen WL, Chandrasekhar J, Madura JD. Comparison of simple potential functions for simulating liquid water. J Chem Phys 1983; 79:926–935.
29. Darden TA, York D, Pedersen LG. Particle mesh Ewald: an N logN method for Ewald sums in large systems. J Chem Phys 1993;98: 10089–10092.
30. Ryckaert JP, Ciccoti G, Berendsen HJC. Numerical integration of the cartesian equations of motion of a system with constraints: molecular dynamics of n-alkanes. J Comput Phys 1977;23:327–341.
31. Ma J, Sigler PB, Xu Z, Karplus M. A dynamic model for the allosteric mechanism of GroEL. J Mol Biol 2000;302:303–313.
32. Rodríguez-Barrios F, Balzarini J, Gago F. The molecular basis of resilience to the effect of the Lys103Asn mutation in non-nucleoside HIV-1 reverse transcriptase inhibitors studied by targeted molecular dynamics simulations. J Am Chem Soc 2005;127:7570–7578.
33. Srinivasan J, Cheatham TE, Cieplak P, Kollman PA, Case DA. Continuum solvent studies of the stability of DNA, RNA and phosphoramidate–DNA helices. J Am Chem Soc 1998;120:9401–9409.
34. Kollman PA, Massova I, Reyes C, Kuhn B, Huo S, Chong L, Lee M, Lee T, Duan Y, Wang W, Donini O, Cieplak P, Srinivasan J, Case DA, Cheatham TE. Calculating structures and free energies of complex molecules: combining molecular mechanics and continuum models. Calculating structures and free energies of complex molecules: combining molecular mechanics and continuum models. Acc Chem Res 2000;33:889–897.
35. Duan Y, Wu C, Chowdhury S, Lee MC, Xiong G, Zhang W, Yang R, Cieplak P, Luo R, Lee T, Caldwell J, Wang J, Kollman P. A point-charge force field for molecular mechanics simulations of proteins based on condensed-phase quantum mechanical calculations. J Comput Chem 2003;24:1999–2012.
36. Lee MC, Duan Y. Distinguishing protein decoys by using a scoring function based on a new AMBER force field, short molecular dynamics simulations, and the generalized Born solvent model. Proteins 2004;55:620–634.
37. Onufriev A, Bashford D, Case DA. A modification of the generalized Born model suitable for macromolecules. J Phys Chem 2000; 104:3712–3720.
38. Sitkoff D, Sharp K, Honig B. Accurate calculation of hydration free energies using macroscopic solvent models. J Phys Chem 1994;98: 1978–1988.
39. Huo S, Massova I, Kollman PA. Computational alanine scanning of the 1:1 human growth hormone-receptor complex. J Comput Chem 2002;23:15–27.
40. Moreira IS, Fernandes PA, Ramos MJ. Computational alanine scanning mutagenesis–an improved methodological approach. J Comput Chem 2007;28:644–654.
41. Gohlke H, Kiel C, Case DA. Insights into protein-protein binding by binding free energy calculation and free energy decomposition for the Ras-Raf and Ras-RalGDS complexes. J Mol Biol 2003; 330:891–913.
42. Holmgren A. Thioredoxin catalyzes the reduction of insulin disulfides by dithiothreitol and dihydrolipoamide. J Biol Chem 1979;254: 9627–9632.
43. Pey AL, Rodríguez-Larrea D, Bomke S, Dammers S, Godoy-Ruiz R, García-Mira M, Sánchez-Ruiz JM. Engineering proteins with tunable thermodynamic and kinetic stabilities. Proteins 2008;71:165–171.
44. Georgescu RE, García-Mira MM, Tasayco ML, Sánchez-Ruiz JM. Heat capacity analysis of oxidized *Escherichia coli* thioredoxin fragments 1-73, 74-108 and their noncovalent complex. Evidence for the burial of apolar surface in protein unfolded states. Eur J Biochem 2001;268:1477–1485.
45. Fernandes PA, Ramos MJ. Theoretical insights into the mechanism for thiol/disulfide exchange. Chemistry 2004;10:257–266.
46. Carvalho AT, Swart M, van Stralen JN, Fernandes PA, Ramos MJ, Bickelhaupt FM. Mechanism of thioredoxin-catalyzed disulfide reduction. Activation of the buried thiol and role of the variable active-site residues. J Phys Chem B 2008;112:2511–2523.
47. Warshel A. Computer simulation of chemical reactions in enzymes and solutions. New York: John Wiley & Sons; 1991. 236 p.
48. Lindahl E, Delarue M. Refinement of docked protein–ligand and protein–DNA structures using low frequency normal mode amplitude optimization. Nucleic Acids Res 2005;33:4496–4506.
49. Mulrooney SB, Williams CH, Jr. Potential active-site base of thioredoxin reductase from *Escherichia coli*: examination of histidine245 and aspartate139 by site-directed mutagenesis. Biochemistry 1994;33:3148–3154.
50. Navarro JA, Gleason FK, Cusanovich MA, Fuchs JA, Meyer TE, Tollin G. Kinetics of electron transfer from thioredoxin reductase to thioredoxin. Biochemistry 1991;30:2192–2195.
51. Negri A, Marco E, Damborsky J, Gago F. Stepwise dissection and visualization of the catalytic mechanism of haloalkane dehalogenase LinB using molecular dynamics simulations and computer graphics. J Mol Graph Model 2007;26:643–651.
52. Li H, Hanson C, Fuchs JA, Woodward C, Thomas GJ, Jr. Determination of the pKa values of active-center cysteines, cysteines-32 and -35, in *Escherichia coli* thioredoxin by Raman spectroscopy. Biochemistry 1993;32:5800–5808.
53. Dillet V, Dyson HJ, Bashford D. Calculations of electrostatic interactions and pKas in the active site of *Escherichia coli* thioredoxin. Biochemistry 1998;37:10298–10306.
54. Marco E, Negri A, Luque FJ, Gago F. Role of stacking interactions in the binding sequence preferences of DNA bis-intercalators: insight from thermodynamic integration free energy simulations. Nucleic Acids Res 2005;33:6214–6224.